Anti-Jamming 5G Millimeter-Wave Communication via Joint Analog and Digital Beamforming: A Bayesian Optimization Approach

Peihao Yan*, Bowei Zhang*, Shichen Zhang*, Kai Zeng†, and Huacheng Zeng*
*Department of Computer Science and Engineering, Michigan State University
†Department of Electrical and Computer Engineering, George Mason University

***Abstract*—5G millimeter-wave (mmWave) communications are essential for enabling ultra-high-speed, low-latency wireless connectivity to support data-intensive applications. However, the highly directional nature and sensitivity of mmWave signals make them particularly susceptible to jamming attacks. As such, securing 5G mmWave communication systems against jamming attacks is critical for ensuring reliable wireless connectivity in mission-critical applications. In this paper, we propose an online Bayesian Optimization (BayOpt) framework for joint analog and digital beamforming optimization at a mmWave communication device, aimed at maximizing its packet decoding rate under a constant jamming attack. By modeling the optimization objective as a black-box function and leveraging online learning to guide beam search, the BayOpt framework efficiently identifies near-optimal beam configurations in both the analog and digital domains while not requiring any knowledge of the jamming strategy or channel conditions. We have implemented the proposed anti-jamming solution on a 28 GHz mmWave testbed and conducted extensive evaluations across four distinct jamming scenarios. Over-the-air experiments demonstrate the effectiveness of the BayOpt framework in suppressing jamming interference. Notably, in a scenario where the jamming signal is 10 dB stronger than the desired signal, the BayOpt-enabled mmWave receiver achieves 73% of the throughput observed in a jamming-free environment.**

***Index Terms*—Bayesian optimization, anti-jamming, mmWave communication, beamforming, online learning**

I. Introduction

5G millimeter-wave (mmWave) technology is crucial for enabling high-speed, low-latency connectivity that supports a wide range of data-intensive applications, including smart cities, autonomous vehicles, and augmented reality. However, the wide applications of 5G mmWave also bring substantial risks. As mmWave links play a crucial role in 5G and beyond, serving as both access links and backbone of cellular network infrastructures, they become attractive targets for malicious actors seeking to disrupt, manipulate, or exploit these systems for their own benefit. Among the myriad threats facing mmWave links, jamming attacks are a significant concern, undermining the reliability and availability of wireless connections and resulting in widespread denial-of-service consequences for applications such as remote surgery, autonomous driving, and other mission-critical applications.

To secure mmWave links against jamming attacks, anti-jamming methods have been proposed in increasingly sophisticated forms, aimed at mitigating or circumventing radio interference caused by unknown sources. Examples of anti-jamming techniques include frequency hopping spread spectrum (FHSS) [1], direct sequence spread spectrum (DSSS) [2], adaptive modulation and coding (AMC) [3], beamforming and directional antennas [4], cognitive radio (CR) [5], jamming detection and nulling [6], game theory-based approaches [7], and other physical-layer security techniques. Despite the large volume of anti-jamming work in the literature, most existing methods were designed for low-frequency (sub-6 GHz) systems and lack experimental validations. The progress in the design of anti-jamming mmWave communication schemes remains very limited [8]. Pioneering works (e.g., [9]–[12]) have studied anti-jamming methods to secure mmWave communications. However, existing work focuses mainly on analytical studies based on ideal channel and system models, providing no experimental validation in realistic scenarios. To the best of our knowledge, the experimental validation of anti-jamming methods for mmWave communication systems has not been explored.

In this paper, we present a beamforming design for a mmWave communication receiver, enabling it to decode data packets in the presence of strong in-band jamming signals. We assume that the receiver has no prior knowledge of the jamming signal—such as its waveform, frame format, or spectral characteristics—and must rely solely on its local operations to suppress the interference and recover the desired signal. The receiver is assumed to be equipped with multiple radio frequency (RF) chains, each connected to a phased-array antenna, enabling it to perform both analog and digital beamforming in the spatial domain. The core of our design is an online Bayesian Optimization (BayOpt) framework for beam search at the mmWave receiver. By treating the optimization objective as a blackbox function and applying online learning to guide the beam search process, the BayOpt framework efficiently identifies near-optimal beam configurations in both analog and digital domains, without requiring any knowledge of the jamming strategy or channel conditions.

To decode data packets in the presence of jamming signals, we face two key challenges. The first challenge lies in the design of digital beamforming (DBF) vectors, which corresponds to signal detection and channel equalization. While DBF has been extensively studied, the uniqueness of our scenario is that the mmWave receiver lacks any knowledge of the jamming channel state information (CSI). Without CSI, it is

unclear how to effectively decode data packets under jamming interference. The second challenge concerns the configuration of analog beamforming (ABF), specifically the selection of a beam from a predefined beambook to optimize communication performance. In practice, the beambook often contains a large number of beam candidates. An exhaustive search through all beam options would be time-consuming and inefficient. Thus, fast beam search algorithms are necessary to identify the optimal beam. Although the literature offers many ABF methods [13]–[16], none address scenarios involving jamming. The problem of efficiently identifying the best beam from a beambook in the presence of jamming signals remains largely unexplored.

The proposed BayOpt framework addresses these two challenges by jointly and iteratively optimizing both analog beamforming and digital beamforming. BayOpt is adopted for two main reasons: (i) The relationship between a selected beam and its achievable data rate under jamming conditions is complex and unknown; and (ii) BayOpt has been shown to be effective for solving optimization problems where the objective function and constraints are unknown and expensive to evaluate. The core idea of the BayOpt framework is to guide beam search using posterior probabilities derived from previously evaluated beams. As more beams are evaluated, the framework gains increasingly accurate information to inform future selections. Compared to exhaustive search, BayOpt is remarkably efficient at identifying near-optimal beams within a given airtime budget.

As a key component of the BayOpt framework, we design a modified minimum mean square error (M-MMSE) detector for DBF. The rationale behind its design is as follows: While the mmWave receiver lacks knowledge about the jamming signals, it does possess knowledge of the desired signal, including its bandwidth, OFDM parameters, and demodulation reference signals (DMRS). Unlike traditional MIMO-based detection methods that estimate channels using DMRS and then apply the estimated channels for payload demodulation, our M-MMSE method bypasses channel estimation. Instead, it directly constructs DBF vectors from the DMRS within a signal frame. This approach not only eliminates the need for intermediate channel estimation but also yields DBF vectors that are effective in mitigating jamming and implicitly equalize the channel for successful signal demodulation.

We have built a prototype of the anti-jamming mmWave receiver device by leveraging the dual polarization (horizontal and vertical) capabilities of a phased-array antenna. The antenna consists of a 4×4 patch element array for analog beamforming and supports two independent data streams for digital beamforming. We evaluated the receiver in a 28 GHz mmWave communication system under various in-band jamming scenarios, aiming to assess its packet decoding rate. Extensive experimental results show that the proposed mmWave receiver achieves, on average, 73% of the throughput compared to jamming-free conditions. A video demonstration of real-time mmWave video streaming in the presence of strong jamming signals is available in [17].

The main contributions of this paper are as follows:

- We design an online Bayesian Optimization framework for joint analog and digital beamforming in a mmWave communication device, enabling robust data decoding under jamming attacks.
- We develop a DBF scheme tailored to the BayOpt framework that effectively mitigates jamming without requiring knowledge of the jamming channel.
- To the best of our knowledge, we are the first to evaluate the proposed BayOpt framework on a 5G mmWave testbed in realistic settings. Extensive experiments confirm its resilience against jamming attacks.

TABLE I: Anti-jamming strategies in the literature.

Type	References	Techniques	Key ideas
Jamming avoidance	[1], [2]	Channel hopping & spreading	FHSS, DSSS, etc.
	[4]	Directional antenna	Use extra spatial info via directional antenna
	[19], [20]	Machine learning	Classify jamming signals for avoidance
Jamming adaptation	[21], [22]	Adaptive beamforming	Beam switching, beam management, and prediction
	[3]	Adaptive modulation	Keep orthogonality to jamming signal
	[23]–[25]	Dynamic resource allocation	Adaptive allocation of power, rate, antennas
	[7], [26], [27]	Game theory	Use game model to compete with jammer
Jamming mitigation	[10], [28]	MIMO	Project signal onto subspace orthogonal to jamming signal
	[29]–[31]	Network coding	Modulation coding, spectrum spreading, phase-coding
	[5], [32]	Cognitive radio	Cooperative Rx to estimate jamming channel
	[11], [33], [34]	Beamforming	ABF/DBF and hybrid beamforming using spatial dimension
	Our work	Analog & digital beamforming	BayOpt ABF and M-MMSE DBF

Conference Version: Part of this paper appeared in IEEE INFOCOM 2023 [18], but it differs significantly from the conference version. The conference paper addresses uplink MU-MIMO mmWave communications in WLAN using Bayesian optimization, while this work focuses on anti-jamming mmWave communication solutions. Experimentally, the conference paper uses planar antennas without beam steering, whereas this work employs phased-array antennas with real-time beam steering.

Acronyms—ABF: Analog Beamforming; AWGN: Additive White Gaussian Noise; BER: Bit Error Rate; BS: Base Station; CDF: Cumulative Distribution Function; CSI: Channel State Information; DBF: Digital Beamforming; DL: Downlink; LoS: Line-of-Sight; MIMO: Multiple-Input Multiple-Output; mmWave: Millimeter Wave; MMSE: Minimum Mean Square Error; MU-MIMO: Multi-User Multiple-Input Multiple-Output; NLoS: Non-Line-of-Sight; O-RAN: Open Radio Access Network; RF: Radio Frequency; SDR: Software-Defined Radio; SNR: Signal-to-Noise Ratio; UL: Uplink.

II. Related Work

Anti-jamming mmWave communication has attracted growing research interest in recent years. Existing approaches can be broadly classified into three main categories: jamming avoidance, jamming adaptation, and jamming mitigation, as summarized in Table I.

Jamming Avoidance: Channel hopping approaches avoid jamming attacks in the frequency domain, requiring large spectrum bands for collision avoidance [1], [2]. These approaches appear to be inefficient due to the spectrum scarcity in real-world systems. Moreover, these approaches need to scan all possible channels to identify a "usable" one, incurring airtime

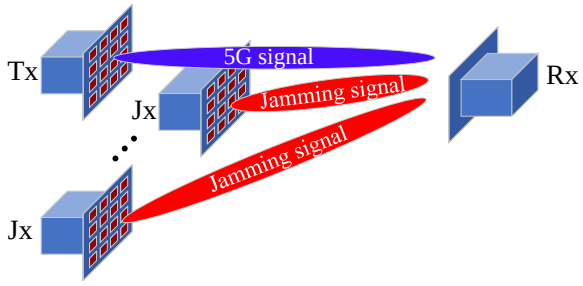

Fig. 1: Threat model.

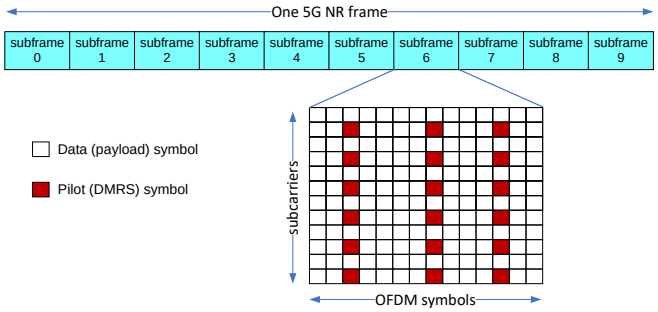

Fig. 2: Illustration of one 5G NR frame structure.

overhead and thus degrading communication efficiency. [4] presents a directional-antenna-based approach for jamming avoidance. However, this approach requires specialized antennas and cannot work in the case where jamming comes from all directions. Recently, machine learning has been studied for jamming detection and avoidance [19], [20]. Our work differs from the above work, as it aims to mitigate jamming signals, rather than avoiding them.

Jamming Adaptation: Adaptive beamforming is a representative approach for jamming adaptation through dynamic beam management. This approach requires sophisticated algorithms for effective beam management [21] and fast beam switching [22]. Another popular approach for jamming adaptation is dynamic resource allocation [24], [25]. This approach is a centralized resource control mechanism to handle various jamming attacks. Despite its potential for adaptability, this approach tends to introduce additional layers of control overhead and raises concerns regarding the equitable distribution of resources. [7], [26], [27] proposed game theory based frameworks that employ reinforcement learning to develop anti-jamming strategies. This approach requires a large amount of datasets for model training, which poses a grand challenge in data acquisition.

Jamming Mitigation: A well-known approach in this class is MIMO-based jamming mitigation, which uses multiple antennas to project received signals onto a subspace orthogonal to the jamming. [10] is a representative work on single-user uplink, where the jammer has a single antenna and the legitimate nodes (base station and user) have antenna arrays. It employs a pilot-hopping protocol within a predefined codebook to guarantee an unused orthogonal pilot sequence. Projecting onto this sequence space allows the base station to estimate both the jammer's and user's channels, enabling reliable decoding under jamming. [31] proposes a physical-layer network coding (PNC) scheme to secure multi-hop communications against jamming. [33] proposed a beamforming approach that leverages spatial information to suppress jamming. The scenario involves a multi-antenna transmitter and receiver, and a single-antenna jammer. The optimization proceeds in two phases: (i) relax the analog beamforming constraint to jointly optimize the product of analog and digital beamforming vectors, and (ii) decompose the product to obtain the individual analog and digital beamforming vectors. [35] proposed a deep learning–based jamming mitigation approach for RIS-NOMA uplink in 5G URLLC applications.

Novelties of This Work: This work falls in the class of jamming mitigation. It differs from the prior work [33], [35] in the following aspects. First, our work focuses on the anti-jamming design for 5G communications, while prior work did not consider the realistic setting (e.g., frame structure) of 5G systems. Second, our work focuses on solution design and experimental validation, while prior work has never implemented and evaluated their anti-jamming solutions in real systems. Instead, prior work relies on simulation or numerical results for evaluation.

III. Problem Description

Consider a mmWave communication network as shown in Figure 1, where a transmitter sends signal frames (data packets) to the receiver in the presence of jamming signals from unknown sources. Both transmitter and receiver are equipped with one or multiple phased-array antennas,[1] allowing them to perform both analog and digital beamformings for signal process. The attacker launches in-band jamming signal emission, which may be strong and time-varying. For simplicity, we assume that the attack is a *constant jamming* throughout the paper. Other types of jamming (e.g., reactive jamming, cognitive jamming, and smart jamming) are out of the scope of this work. In the presence of constant jamming attacks, an existing mmWave receiver is incapable of decoding its data packets, resulting in a communication disruption. Our objective is to design a new mmWave receiver that secures mmWave communications against constant in-band jamming attacks.

A. Problem Formulation

5G Frame Structure: In 5G new radio (NR) communications, the signal transmission is structured in frames as shown in Figure 2. A 5G NR frame encompasses a sequence of subframes of the same length. Each subframe comprises an array of OFDM symbols, expanding to its frequency band over subcarriers. Combining the temporal (over OFDM symbols) and spectral (over OFDM subcarriers) domains, the resource can be formatted to a two-dimensional grid, as shown in Figure 2. Each small box is called a resource element (RE). A set of adjacent REs are grouped (e.g., 7 OFDM symbols by

[1]As we will show in the implementation section, when the mmWave device has a single phased-array antenna, it can support two data streams for digital beamforming by utilizing the antenna's dual (horizontal and vertical) polarization.

12 OFDM subcarriers) and called resource block (RB), which is the basic unit for data transmission and reception. Over the resource grid, a subset of REs are selected for Demodulation Reference Signal (DMRS), which is used for a receiver to estimate channel and demodulate signal. To the end, we will show that these DMRS REs will play a critical role in jamming mitigation at the receiver.

Analog Beamforming (ABF): Due to the high frequency of mmWave, signal power attenuates rapidly over its travel distance. ABF is used to steer radio energy to a specific direction, such that the communication range can be extended while maintaining a low cost and low power of RF hardware. In practice, a phased-array antenna has multiple patch elements. A vector of weights, each of which is a complex number corresponding to the amplitude amplifying factor and phase shifter, is used to steer the beam direction in both horizontal and vertical planes. This weight vector is called ABF vector. In real systems, the ABF vectors are typically predefined, each corresponding to a beam direction. With the predefined beambook, ABF boils down to beam selection, namely selecting the best beam in a predefined beambook to optimize a given objective (e.g., maximizing throughput). In this work, we focus on the fast beam selection from a given beambook, rather than the design of beamforming weights.

Referring to the threat model in Figure 1, we assume there is a single transmitter and $(N-1)$ jammers. Denote s as the signal from the transmitter and $[z_2, z_3, \ldots, z_N]$ as the jamming signals. Denote $\tilde{\mathbf{H}}_n$ as the over-the-air channels from transmitter/jammer to receiver. Denote $\vec{a}_1$ as the ABF vector at the transmitter and $\vec{a}_n$, $2 \leq n \leq N$, as the ABF vector at the jammer. Denote M as the number of receiver's antennas. Denote $\mathcal{B} = \{\vec{\theta}_1, \vec{\theta}_2, \cdots, \vec{\theta}_B\}$ as the set of predefined beambook for ABF. Denote $\vec{\theta} = [\vec{b}_1, \vec{b}_2, \ldots, \vec{b}_M]$ as the aggregated ABF at the receiver, where $\vec{b}_m \in \mathcal{B}$ for $1 \leq m \leq M$. Denote $\vec{b}_m \in \vec{\theta}$ as the ABF vector for the mth antenna at the receiver. Then, we have:

$$y_m = \vec{b}_m^{\top}\Big(\underbrace{\tilde{\mathbf{H}}_1\vec{a}_1 s}_{signal} + \underbrace{\sum_{n=2}^{N}\tilde{\mathbf{H}}_n\vec{a}_n z_n}_{jamming}\Big) + w_m, \tag{1}$$

where w_m is the noise at receiver's mth antenna. We note that the receiver has no knowledge of the jammer, including (i) the over-the-air jamming channel $\tilde{H}_n$, $1 \leq n \leq N$, and (ii) the jamming beamforming vector $\vec{a}_n$, $1 \leq n \leq N$. Therefore, the receiver design must be carried out without either of these pieces of information.

Digital Beamforming (DBF): When a mmWave device has two or more digital chains, DBF can be applied to the baseband. In our work, the DBF at receiver is exploited for two purposes: *jamming mitigation* and *signal detection*. Denote $\vec{p}$ as the DBF vector. Then, the DBF operation can be written as:

$$\hat{s} = \vec{p}^{\top}\vec{y}, \tag{2}$$

where $\hat{s}$ is the estimated version of original signal s and $\vec{y} = [y_1, y_2, \ldots, y_M]^{\top}$.

Objective Function: We assume that the ABF and DBF at the transmitter and jammer are given. We focus on the design of ABF and DBF at the receiver. We define the objective function as the error vector magnitude (EVM) at the receiver because EVM can relect reliability and performance of the entire communication system. Mathematically, we define: $f(\vec{\theta}, \vec{p}) = \frac{\mathbb{E}[|s-\hat{s}|^2]}{\mathbb{E}[|s|^2]}$. Then, based on Equations (1) and (2), the beamforming optimization problem can be written as:

$$[\vec{\theta}^*, \vec{p}^*] = \arg\min_{\vec{\theta}\in\mathcal{B},\vec{p}} f(\vec{\theta}, \vec{p}) = \arg\min_{\vec{\theta}\in\mathcal{B},\vec{p}}\Big(\frac{\mathbb{E}[|s-\hat{s}|^2]}{\mathbb{E}[|s|^2]}\Big). \tag{3}$$

B. Challenges

Solving the optimization problem in (3) is challenging for the following reasons.

Unknown Jamming Waveform: The receiver has no knowledge about jamming signals $[z_2, z_3, \ldots, z_N]$. The jamming signal can be any waveform, such as OFDM, CDMA, and noise. Additionally, the spectrum of jamming signals may be partially or fully overlapping with the spectrum of the desired signal. The unknown structure of jamming signals calls for a blind jamming mitigation strategy for signal detection.

Unknown Jamming Channels: Due to the lack of knowledge regarding jamming signals, it is hard to obtain the channel knowledge between the jammer and the receiver, i.e., $\tilde{\mathbf{H}}_n$ for $2 \leq n \leq N$. Additionally, receiver does not have knowledge about the ABF vectors at jammer. The lack of channel knowledge makes it challenging to design efficient ABF and DBF vectors at receiver.

Coupling of ABF and DBF: It is easy to see that the ABF design over the receiver's multiple antennas is tightly coupled with each other. Optimizing ABF for individual antennas does not lead to an optimal or near-optimal solution. In addition, the ABF and DBF are coupled as well. This calls for a joint ABF and DBF design at the receiver.

IV. Design Overview

In this section, we propose a BayOpt framework for the mmWave device's joint ABF and DBF optimization. BayOpt is an online learning framework. It is a model-free, end-to-end solution requiring no knowledge about antenna and channel models, such as jammer's channel $\tilde{H}_n$ and beamforming vector $\vec{a}_n$ in Eqn (1).

A. Our Approach

Online Learning Framework: ABF is to find the optimal or near-optimal beam index in a predefined beambook so as to maximize the data rate (equivalently, minimizing EVM) at the mmWave receiver device. In practice, the beambook is typically large. For instance, if the predefined beambook has 60 horizon angles and 60 elevation angles. Then, the beambook has 3600 beam candidates. On one hand, an exhaustive search is too costly for practical use. It entails a large airtime overhead and thus compromises communication efficiency. On the other hand, while the literature has efficient beam search strategies (e.g., compressive sensing [36], [37]), most of them aim to maximize the signal strength of each individual antenna. It is

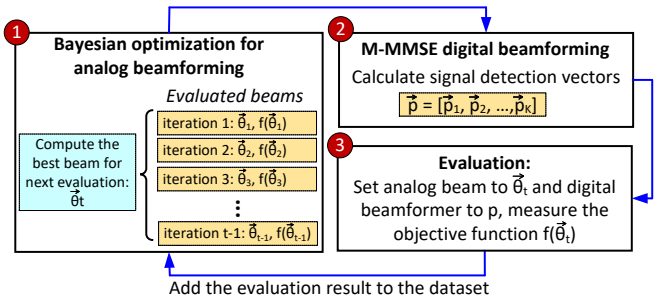

Fig. 3: The high-level system diagram.

not suited for the case where jamming presents because they cannot differentiate jamming and useful signals.

To tackle this problem, we employ a BayOpt scheme for joint beam search. BayOpt has been proved to be an effective technique for solving sequential optimization problems where the objective function is complex (treated as a black-box), the (sub-)gradient is unknown, and the evaluation is expensive [38]. To illustrate the idea behind BayOpt, let us consider the beams in a beambook $[\vec{\theta}_1, \vec{\theta}_2, \ldots, \vec{\theta}]$, among which we intend to find a beam to minimize the objective function $f(\vec{\theta})$. Suppose that we have measured two beams, say $\vec{\theta}_{10}$ and $\vec{\theta}_{1000}$, and found that $f(\vec{\theta}_{10}) = 5$ and $f(\vec{\theta}_{1000}) = 0.1$. Then, in the next iteration, we should select a beam in the neighborhood of $\vec{\theta}_{1000}$ to evaluate, because the global minimum is more likely sitting in the neighborhood of $\vec{\theta}_{1000}$ compared to $\vec{\theta}_{10}$. Through a principled strategy, BayOpt guides the process of joint beam search based on posterior probability.

Adaptive Digital Beamforming (DBF): DBF plays a crucial role in jamming mitigation. Unlike conventional MIMO-based signal detection, which mitigates inter-user interference to recover intended signal streams, DBF in this scenario faces the challenge of operating without CSI. Without CSI, existing MIMO detectors such as zero-forcing or MMSE cannot be applied. To overcome this challenge, we design a modified MMSE (M-MMSE) DBF scheme to mitigate unknown jamming signals for useful signal decoding.

B. System Diagram

Figure 3 shows the system diagram for our proposed anti-jamming scheme. The Rx measures the performance of a sequence of analog beams $[\vec{\theta}_1, \vec{\theta}_2, \ldots, \vec{\theta}_t, \ldots, \vec{\theta}_T]$, where t is the iteration index and T is the predefined maximum number of iterations allowed (e.g., $T = 30$). In the end of T iterations, the mmWave Rx device chooses the beam that yields the best performance (i.e., yielding the minimum EVM value). In each iteration t, the operations include the following three steps:

- **Step 1**: The Rx selects a beam $\vec{\theta}_t$ for evaluation in the current iteration (i.e., iteration t) based on the posterior probability derived from the past evaluations, i.e., $(\vec{\theta}_{t'}, f(\vec{\theta}_{t'}))$ for $1 \leq t' < t$. Our method of selecting $\vec{\theta}_t$ from the beambook based on the knowledge generated from prior evaluations is presented in Section V.
- **Step 2**: After choosing the analog beam $\vec{\theta}_t$, the Rx calculates its DBF vectors $\vec{p}$ for each resource block in the OFDM frame. Using these DBF vectors (a.k.a., signal detection filters), the Rx starts to decode the signal frames from the Tx in the presence of jamming signals. Our method of designing DBF vectors is presented in Section VI.
- **Step 3**: Rx measures the EVM of decoded signals. By doing so, it obtains $f(\vec{\theta}_t)$. Then, $(\vec{\theta}_t, f(\vec{\theta}_t))$ is added to the dataset and will be used to guide the future beam search.

V. A Bayesian Optimization Framework

In this section, we present the BayOpt design to find a near-optimal beam $\vec{\theta}$ from a given beambook for the Rx. The design of digital beamforming vector $\vec{p}$ will be presented in the next section.

A. Why Bayesian Optimization?

The objective is to solve the optimization problem $\arg\min f(\vec{\theta})$, where $\vec{\theta} \in \mathcal{B}$. However, $f(\vec{\theta})$ is a complex function and cannot be solved analytically. It has the following features.

- *$f(\vec{\theta})$ has a complex structure:* Consider the ABF problem at an anti-jamming Rx. Denote $\vec{\theta}$ as a beam direction from the beambook. Let $f(\vec{\theta})$ be the measured EVM at the Rx. Figure 4 shows an example of $f(\vec{\theta})$ obtained through exhaustive beam search on our mmWave testbed in the presence of jamming signals[2]. It is evident that $f(\vec{\theta})$ is an irregular non-convex function. It is nontrivial, if even possible, to solve it analytically.
- *$f(\vec{\theta})$ is unknown:* The presence of time-varying jamming signals, makes it extremely hard to model $f(\vec{\theta})$.
- *Evaluating $f(\vec{\theta})$ is costly:* To evaluate $f(\vec{\theta})$ for a given $\vec{\theta}$, the Rx needs to physically set up the beam pattern and measure the resultant signal quality. This process incurs non-negligible airtime overhead.

Fortunately, BayOpt is an effective technique to optimize a function that is unknown yet expensive to evaluate [38]. It makes use of the laws of probability to combine prior belief with observed data to compute posterior distribution of the objective function. Therefore, we will design a BayOpt framework for analog beam search.

B. A Bayesian Optimization Framework

To perform BayOpt, one needs to address two problems: i) finding a statistical process to model the function being optimized, and ii) selecting an acquisition function as a surrogate approximation to guide the search in each iteration. In what follows, we address these two problems in order.

Gaussian Process Regression (GPR): We model the iterative beam search problem as a Gaussian process. The reasons are as follows:

- Beam search problem involves complex, non-linear relationship. GPR allows flexibility in choosing kernel functions. Different kernels can capture different types

[2]The detailed experimental setup is presented in Section VIII-A.

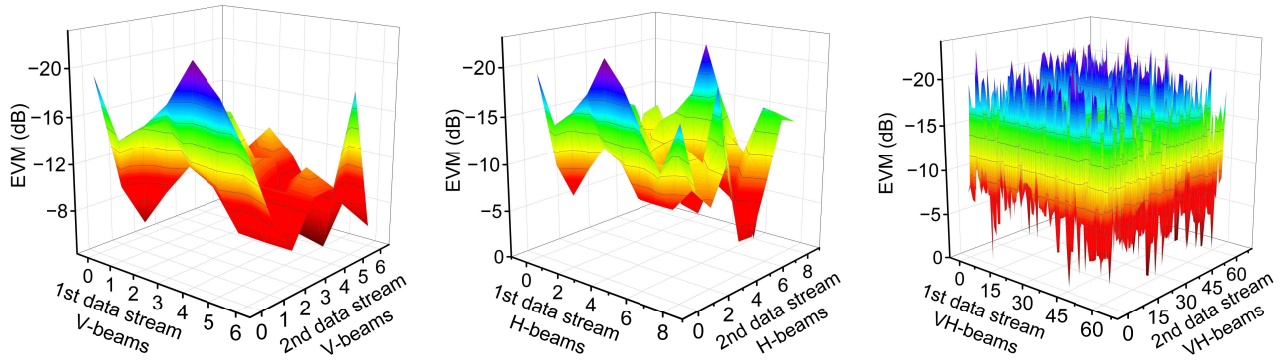

(a) Measured EVM vs. vertical beams.

(b) Measured EVM vs. horizontal beams.

(c) Measured EVM vs. vertical and horizontal beams.

Fig. 4: Measured EVM values at a mmWave receiver when it demodulates signals in the presence of jamming signals. The x-axis and y-axis labels represent the beam index.

of relationship, adapting to the different characteristics of the beam search problem.

- GPR provides not only predictions but also estimates of uncertainty with these predictions. It can guide beam search by indicating the variety due to environmental conditions.
- Beam search problems often involve sparse data points, which limits direct measurements or simulations. While GPR can effectively interpolate between sparse data points, providing reliable predictions with a small number of observation.

In the tth iteration, the Rx has observed $t-1$ beams. Denote $\mathbf{\Theta} = \{\vec{\theta}_i\}_{i=1}^{t-1}$ as the set of beams that the Rx has already observed. Denote $f(\mathbf{\Theta}) = \{f(\vec{\theta}_i)\}_{i=1}^{t-1}$ as the objective function values of those observed beams. We treat $f(\mathbf{\Theta})$ as a multi-variate Gaussian distribution, with $\mu(\mathbf{\Theta})$ as its mean and $k(\mathbf{\Theta},\mathbf{\Theta})$ as its covariance kernel. Here, $\mu(\mathbf{\Theta})$ is a $(t-1)\times 1$ vector, while $k(\mathbf{\Theta},\mathbf{\Theta})$ is a $(t-1)\times(t-1)$ matrix. Let $\vec{\theta}$ be an arbitrary beam in the beambook. Then, per the definition of Gaussian process, the joint distribution of the function values corresponding to $\vec{\theta}$ and $\mathbf{\Theta}$ should satisfy:

$$\begin{bmatrix} f(\mathbf{\Theta}) \\ f(\vec{\theta}) \end{bmatrix} \sim \mathcal{N}\left(\begin{bmatrix} \mu(\mathbf{\Theta}) \\ \mu(\vec{\theta}) \end{bmatrix}, \begin{bmatrix} k(\mathbf{\Theta},\mathbf{\Theta}) & k(\mathbf{\Theta},\vec{\theta}) \\ k(\vec{\theta},\mathbf{\Theta}) & k(\vec{\theta},\vec{\theta}) \end{bmatrix} \right), \quad (4)$$

where $\mu(\cdot)$ and $k(\cdot,\cdot)$ should be understood as an element-wise operational function. There are various definitions for Gaussian kernel, such as *Matérn* kernel, *exponentiated quadratic* kernel, and *radial basis function* kernel [39]. In our experiments, we choose radial basis function kernel, $k(\vec{\theta}_i,\vec{\theta}_j) = \exp(-\frac{1}{2\sigma^2}\|\vec{\theta}_i - \vec{\theta}_j\|^2)$, where σ is a hyper-parameter that governs the kernel width. In our experiments, we let $\sigma = 1$.

The posterior distribution on the arbitrary beam $\vec{\theta}$ can be calculated through standard Bayesian rules. Specifically, the distribution of $f(\vec{\theta})$ can be modeled as:

$$f(\vec{\theta}) \sim p\big(f(\vec{\theta})|\vec{\theta},\mathbf{\Theta},f(\mathbf{\Theta})\big) = \mathcal{N}\big(\mu(\vec{\theta}),\Sigma(\vec{\theta})\big), \quad (5)$$

where

$$\mu(\vec{\theta}) = k(\vec{\theta},\mathbf{\Theta})k(\mathbf{\Theta},\mathbf{\Theta})^{-1}f(\mathbf{\Theta}), \quad (6)$$

$$\Sigma(\vec{\theta}) = k(\vec{\theta},\vec{\theta}) - k(\vec{\theta},\mathbf{\Theta})k(\mathbf{\Theta},\mathbf{\Theta})^{-1}k(\mathbf{\Theta},\vec{\theta}). \quad (7)$$

Acquisition Function: There are different acquisition functions available for BayOpt problems such as Probability of Improvement (PoI), Expected Improvement (EI), and Gaussian process Upper Confidence Bound (GP-UCB) [39]. We choose EI for two reasons: i) compared to PoI, it has been shown to be better-behaved; and ii) unlike GP-UCB, it does not involve tuning parameters [40]. The acquisition function can be written as:

$$\mathrm{EI}(\vec{\theta}) = \mathbb{E}\big[\max(f(\vec{\theta}) - f(\vec{\theta}^+),0)\big], \quad (8)$$

where $\vec{\theta}^+$ is the best beam found so far. Under the Gaussian process model, it can be analytically written as follows:

$$\mathrm{EI}(\vec{\theta}) = \big(\mu(\vec{\theta}) - f(\vec{\theta}^+) - \xi\big)\,\mathrm{CDF}(Z) + \Sigma(\vec{\theta})\,\mathrm{pdf}(Z), \quad (9)$$

where $Z = \frac{\mu(\vec{\theta})-f(\vec{\theta}^+)-\xi}{\Sigma(\vec{\theta})}$, $\mathrm{CDF}(\cdot)$ and $\mathrm{pdf}(\cdot)$ are the cumulative distribution function and the probability density function of standard normal distribution, respectively, and ξ is a parameter that determines the amount of exploration during the optimization. A large value of ξ leads to more exploration, while a small value leads to more exploitation. In our experiments, we empirically set ξ to 0.1.

Beam Selection: Then, in the tth iteration, the beam selected for evaluation is obtained by solving the following problem:

$$\vec{\theta}_t = \underset{\vec{\theta}\in\mathcal{B}\setminus\mathbf{\Theta}}{\arg\max}\ \mathrm{EI}(\vec{\theta}), \quad (10)$$

where $\mathcal{B}$ is the set of all predefined beams and $\mathbf{\Theta}$ is the set of beams that have been evaluated so far. It is worth noting that (10) is easy to solve because (9) is a simple, disciplined function.

C. Practical Considerations

There are two challenges associated with the above BayOpt framework when it is applied to beam search. In the following, we first point out the challenges and then present our solutions.

Limited Number of Evaluations: MmWave systems have a fixed airtime budget for beam search/training, which deter-

mines the maximum number of evaluations/iterations that can be performed before data transmission. In practice, given the limited airtime budget for beam search, it may not be able to find the optimal beam for data transmission. Therefore, the beam search problem is further constrained by the number of evaluations. To address this challenge, we propose a *recenter-and-shrink* (RaS) scheme for the Gaussian process regression. This scheme was inspired by [41]. The basic idea is that, when approaching the evaluation budget, we *recenter* the search space to the current optimal beam and *shrink* the search space. Doing so increases the probability of finding a better beam when we reach the evaluation budget. Following this idea, we modify the acquisition function in (10) to:

$$\vec{\theta}_t = \underset{\vec{\theta}\in\mathcal{B}\setminus\mathbf{\Theta}}{\arg\max}\ \mathrm{EI}(\vec{\theta}) \tag{11}$$
$$\text{s.t. } \theta_m \in \begin{cases} [-\frac{\pi}{2},\ \frac{\pi}{2}] & \text{if } 1 \le t < T/2 \\ [\theta_m^+ - \frac{\phi_t}{2},\ \theta_m^+ + \frac{\phi_t}{2}] & \text{if } T/2 \le t \le T. \end{cases}$$

where t is the iteration/evaluation index, T is the maximum number of evaluations, $\vec{\theta}^+ = [\theta_m^+]_{m=1}^M$ is the best beam found so far, and ϕ_t is the reduced search range. Empirically, we set $\phi_t = (\frac{3}{2} - \frac{t}{T})\pi$ in our experiments.

Cubic Computational Complexity: The computational complexity of Gaussian process regression is cubic to the number of data samples, i.e., $\mathcal{O}(t^3)$, where t is the number of evaluations that have been performed. Rank-1 updates are typically used to compute matrix inverse in a more efficient manner, i.e., $\mathcal{O}(t^2)$. Clearly, the computation rapidly increases as the evaluation procedure evolves. To overcome the computation challenge of Gaussian process, a wealth of sparse approximations have been recently suggested, such as the subset of data (SoD) approximation, the subset of regressors (SoR) approximation, the deterministic training conditional (DTC) approximation, and partially independent training conditional (PITC) approximation [42]. *In these methods, a subset of the latent variables are treated exactly while the remaining variables are treated approximately to reduce the computation.* Here, we employ the SoR approximation for the beam search as it demonstrates a good tradeoff between performance and computation (see Tables 8.1 & 8.2 in [42]).

Denote $\mathbf{\Phi}$ as the subset of training data samples that are selected for exact regression, where $\mathbf{\Phi} \subset \mathbf{\Theta}$. Per [42], the Gaussian process regression can be characterized by the approximate mean and covariance as follows:

$$\mu(\vec{\theta}) = \sigma^{-2} k(\vec{\theta}, \mathbf{\Phi}) \mathbf{Q}^{-1} k(\mathbf{\Phi}, \mathbf{\Theta}) f(\mathbf{\Theta}), \tag{12}$$
$$\Sigma(\vec{\theta}) = k(\vec{\theta}, \mathbf{\Phi}) \mathbf{Q}^{-1} k(\mathbf{\Phi}, \vec{\theta}), \tag{13}$$

where $\mathbf{Q} = \sigma^{-2} k(\mathbf{\Phi}, \mathbf{\Theta}) k(\mathbf{\Theta}, \mathbf{\Phi}) + k(\mathbf{\Phi}, \mathbf{\Phi})$.

A question to ask is how to select the active data samples for $\mathbf{\Phi}$. Empirically, we define an integer number $\tau \in \mathbb{Z}$ which is smaller than t. We choose the τ beams in $\mathbf{\Theta}$ that are closest to $\vec{\theta}^+$ as the active samples for $\mathbf{\Phi}$. Denote $g(\vec{\theta}) \triangleq \|\vec{\theta}^+ - \vec{\theta}\|^2$ as the metric for $\vec{\theta}$. Based on this metric, we sort the elements in $\mathbf{\Theta}$ in a non-decreasing order and denote the resulting vector as $\mathbf{\Theta}_{srt} = [\vec{\theta}_{s_1}, \vec{\theta}_{s_2}, \cdots, \vec{\theta}_{s_t}]$. Then, we let:

$$\mathbf{\Phi} = [\vec{\theta}_{s_1}, \vec{\theta}_{s_2}, \cdots, \vec{\theta}_{s_\tau}]. \tag{14}$$

Algorithm 1 Bayesian optimization for analog beam search

Required: T: the budgeted number of evaluations.
Output: A beam $\vec{\theta}^*$ in the predefined beambook $\mathcal{B}$ for data packet reception at the Rx
Initialization $\mathbf{\Theta} = [\vec{0}]$.
for $t = 1, 2, \cdots, T$ **do**
  Calculate $\mathbf{\Phi}$ using (14)
  Calculate $\mu(\vec{\theta})$ using (12) and $\Sigma(\vec{\theta})$ using (13)
  Construct the surrogate function $\mathrm{EI}(\vec{\theta})$ using (9)
  Find the next beam direction $\vec{\theta}_t$ by solving (11)
  Add $\vec{\theta}_t$ to $\mathbf{\Theta}$
end for
return $\vec{\theta}^* = \arg\min_{\vec{\theta}\in\mathbf{\Theta}} f(\vec{\theta})$.

With the approximation in (12)-(14), the computational complexity of Gaussian process regression in the tth iteration decreases to $\mathcal{O}(\tau^2 t)$. More importantly, the complexity scales linearly (rather than cubically) with the number of iterations.

We present the proposed BayOpt algorithm in Alg. 1. In a nutshell, it is a non-parametric online learning algorithm that guides the beam search using the posterior probability of those data samples that have been evaluated so far.

Convergence: By modeling the beam–throughput relationship with Gaussian Process Regression, our BayOpt method predicts both the expected performance and the uncertainty of unexplored beams. This enables the acquisition function to balance exploration of new beam directions with exploitation of promising regions, rapidly narrowing the search to high-performing areas without the need for exhaustive testing. Our practical enhancements, such as the recenter-and-shrink strategy, which focuses the search space as the iteration budget is consumed, and the subset-of-regressors approximation, which reduces the computational complexity of Gaussian process regression, further accelerate convergence. As we will show in our experiments, the proposed approach attains near-optimal beam configurations in only a small fraction of the time required by exhaustive search.

VI. Digital Beamforming for Jamming Mitigation

In this section, we focus on the design of DBF vectors, i.e., $\vec{p} = [\vec{p}_1, \vec{p}_2, \ldots, \vec{p}_K]$, where K is the number of subcarriers in the OFDM modulation and $\vec{p}_k \in \mathbb{C}^{M\times 1}$ with M being the number of antennas on the Rx. In what follows, we first review classic MMSE MIMO detector and then show that a modification of the classic MMSE MIMO detector can eliminate the need for CSI. More importantly, the modified MMSE MIMO detector is capable of decoding useful signals in the presence of jamming signals.

A. Review of Classic MMSE MIMO Detector

Consider an MIMO transmission from an N-antenna Tx to an M-antenna Rx. Suppose that $N \le M$. Then, the signal transfer model in the digital domain (on a single subcarrier) can be written as:

$$\vec{y} = \mathbf{H}\vec{x} + \vec{w}, \tag{15}$$

where $\vec{y} \in \mathbb{C}^{M\times 1}$ is the received digital baseband signal vector at the Rx, $\vec{x} = [x_1, x_2, \ldots, x_N]^\top$ is the transmit signal vector, where x_n is the signal carried by the nth stream, $\vec{w} \in \mathbb{C}^{M\times 1}$ is the noise vector, and $\mathbf{H} = [H_{mn}]_{1\le m\le M, 1\le n\le N} \in \mathbb{C}^{M\times N}$ is the compound channel between the Tx and the Rx.

To decode the N data packets, the Rx can first estimate the compound channel using the reference signals and then construct the MMSE MIMO detector as follows:

$$\mathbf{P} = \mathbf{H}^{\mathsf{H}}(\mathbf{H}\mathbf{H}^{\mathsf{H}} + \frac{\sigma_w^2}{\sigma_x^2}\mathbf{I})^{-1}, \tag{16}$$

where $\mathbf{I}$ is an identity matrix of proper dimension, σ_x^2 is signal power, and σ_w^2 is noise power. After computing MMSE detector, the Rx can perform MIMO detection as follows: $\hat{\vec{x}} = \mathbf{P}\vec{y}$, where $\hat{\vec{x}}$ is an estimated copy of $\vec{x}$. It is then sent to the downstream pipeline for signal demodulation.

This decoding method cannot work for a receiver in the presence of jamming signals, because it does not have the channel knowledge, i.e., $\mathbf{H}$ in Equation (16). In the following, we present a modified MMSE detector for anti-jamming signal detection.

B. Modified MMSE MIMO Detector

In the case of anti-jamming communications, the received signal vector (on a single subcarrier in an OFDM symbol) can be written as follows.

$$\vec{y} = \begin{bmatrix} y_1 \\ y_2 \\ \vdots \\ y_M \end{bmatrix} = \begin{bmatrix} H_{11} & H_{12} & \ldots & H_{1N} \\ H_{21} & H_{22} & \ldots & H_{2N} \\ \vdots & \vdots & \vdots & \vdots \\ H_{M1} & H_{M2} & \ldots & H_{MN} \end{bmatrix} \begin{bmatrix} s \\ z_2 \\ \vdots \\ z_N \end{bmatrix} + \begin{bmatrix} w_1 \\ w_2 \\ \vdots \\ w_M \end{bmatrix}, \tag{17}$$

where s is the desired signal and z_n, $n = 2, 3, \ldots, N$, is the jamming signal. In total, there are $(N-1)$ jamming signal streams. w_m is the noise received on the mth antenna at the Rx. For simplicity, we denote $\vec{x} = [s, z_2, \ldots, z_N]^\top$ as the signal vector on the Tx/Jx side.

It can be clearly seen that the computation of MMSE detector in (16) needs channel matrix $\mathbf{H}$. In the presence of jamming signals, the Rx will not be able to estimate the channel matrix using the DMRS embedded in the frame, posing a grand challenge in signal detection. To address this challenge, we modify the MMSE detector in (16). It turns out that the modified MMSE detector does not need CSI (channel matrix). More notably, it is capable of decoding the desired signal in the presence of unknown jamming signals.

Denote $\mathcal{F}\{\cdot\}$ as an operator that returns the first row of a matrix or the first element of a vector. Denote $\hat{s}$ as the estimate of original signal s. Recall that $\hat{\vec{x}} = \mathbf{P}\vec{y}$ is signal detection operation in the classic MMSE detection. Per the classic MMSE detection, we have

$$\hat{s} = \mathcal{F}\{\hat{\vec{x}}\} = \mathcal{F}\{\mathbf{P}\vec{y}\} = \mathcal{F}\{\mathbf{P}\}\vec{y}. \tag{18}$$

Denote $\mathbf{R}_x$ as the correlation matrix of $\vec{x}$, i.e., $\mathbf{R}_x = \mathbb{E}[\vec{x}\vec{x}^{\mathsf{H}}]$. Denote $\mathbf{R}_w$ as the correlation matrix of $\vec{w}$, i.e., $\mathbf{R}_w = \mathbb{E}[\vec{w}\vec{w}^{\mathsf{H}}]$. Per (16), we have

$$\begin{aligned}
\mathcal{F}\{\mathbf{P}\} &= \mathcal{F}\Big\{\mathbf{H}^{\mathsf{H}}(\mathbf{H}\mathbf{H}^{\mathsf{H}} + \frac{\sigma_w^2}{\sigma_x^2}\mathbf{I})^{-1}\Big\} \\
&\overset{(a)}{=} \mathcal{F}\Big\{\mathbf{R}_x\mathbf{H}^{\mathsf{H}}(\mathbf{H}\mathbf{R}_x\mathbf{H}^{\mathsf{H}} + \mathbf{R}_w)^{-1}\Big\} \\
&= \mathcal{F}\Big\{\mathbb{E}[\vec{x}\vec{x}^{\mathsf{H}}]\mathbf{H}^{\mathsf{H}}(\mathbf{H}\mathbb{E}[\vec{x}\vec{x}^{\mathsf{H}}]\mathbf{H}^{\mathsf{H}} + \mathbb{E}[\vec{w}\vec{w}^{\mathsf{H}}])^{-1}\Big\} \\
&= \mathbb{E}\Big[\mathcal{F}\{\vec{x}\vec{x}^{\mathsf{H}}\mathbf{H}^{\mathsf{H}}\}\Big]\mathbb{E}\Big[\mathbf{H}\vec{x}\vec{x}^{\mathsf{H}}\mathbf{H}^{\mathsf{H}} + \vec{w}\vec{w}^{\mathsf{H}}\Big]^{-1} \\
&= \mathbb{E}\Big[\mathcal{F}\{\vec{x}\}\vec{x}^{\mathsf{H}}\mathbf{H}^{\mathsf{H}}\Big]\mathbb{E}\Big[\mathbf{H}\vec{x}\vec{x}^{\mathsf{H}}\mathbf{H}^{\mathsf{H}} + \vec{w}\vec{w}^{\mathsf{H}}\Big]^{-1} \\
&= \mathbb{E}\Big[s(\mathbf{H}\vec{x})^{\mathsf{H}}\Big]\mathbb{E}\Big[(\mathbf{H}\vec{x} + \vec{w})(\mathbf{H}\vec{x} + \vec{w})^{\mathsf{H}}\Big]^{-1} \\
&\overset{(b)}{=} \mathbb{E}\Big[s(\mathbf{H}\vec{x} + \vec{w})^{\mathsf{H}}\Big]\mathbb{E}\Big[(\mathbf{H}\vec{x} + \vec{w})(\mathbf{H}\vec{x} + \vec{w})^{\mathsf{H}}\Big]^{-1} \\
&= \mathbb{E}\big[s\vec{y}^{\mathsf{H}}\big]\mathbb{E}\big[\vec{y}\vec{y}^{\mathsf{H}}\big]^{-1},
\end{aligned} \tag{19}$$

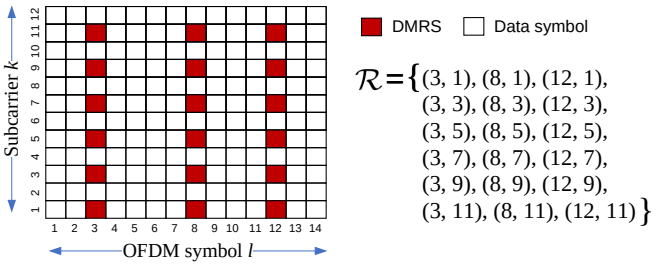

Fig. 5: Illustrating set $\mathcal{R}$ for a RB in 5G NR frame.

where (a) and (b) follow from the assumptions that $\mathbf{R}_x$ is of full rank and $\mathbb{E}[x_n\vec{w}] = 0$, respectively. Both assumptions are valid in practice.

It is evident that the modified MMSE detector presented in Eq. (19) does not need channel knowledge $\mathbf{H}$. Instead, it uses $\mathbb{E}[s\vec{y}^{\mathsf{H}}]$ and $\mathbb{E}[\vec{y}\vec{y}^{\mathsf{H}}]$ to replace the channel matrices. Now the question to ask is how to compute these two terms. In our design, we use the sample averaging operation to approach the statistical expectation based on the fact that every subframe in 5G frame structure has DMRS. Consider a specific resource block (RB) in 5G NR frame. Denote $\mathcal{R}$ as the set of DMRS in the resource block, as shown in Figure 5. Denote l and k as the index of OFDM symbol and subcarrier in a resource block, respectively. Then, we approach $\mathbb{E}[s\vec{y}^{\mathsf{H}}]$ and $\mathbb{E}[\vec{y}\vec{y}^{\mathsf{H}}]$ via approximation as follows: $\mathbb{E}[s\vec{y}^{\mathsf{H}}] \triangleq \sum_{(l,k)\in\mathcal{R}} s(l,k)\vec{y}(l,k)^{\mathsf{H}}$ and $\mathbb{E}[\vec{y}\vec{y}^{\mathsf{H}}] \triangleq \sum_{(l,k)\in\mathcal{R}} \vec{y}(l,k)\vec{y}(l,k)^{\mathsf{H}}$.Consequently, the DBF vector that the Rx uses to decode the data symbols in this resource block can be expressed as:

$$\begin{aligned}
\mathcal{F}\{\mathbf{P}\} &\overset{(19)}{=} \mathbb{E}[s\vec{y}^{\mathsf{H}}]\mathbb{E}[\vec{y}\vec{y}^{\mathsf{H}}]^{-1} \\
&\triangleq \Big[\sum_{(l,k)\in\mathcal{R}} s(l,k)\vec{y}(l,k)^{\mathsf{H}}\Big]\Big[\sum_{(l,k)\in\mathcal{R}} \vec{y}(l,k)\vec{y}(l,k)^{\mathsf{H}}\Big]^{\dagger},
\end{aligned} \tag{20}$$

where $(\cdot)^\dagger$ is the pseudo-inverse operator, and $s(l,k)$ and $\vec{y}(l,k)$ represent the transmitted and received reference signal on OFDM symbol l and subcarrier k, respectively.

C. Performance Analysis

Given its generality, it is extremely hard to analytically characterize the performance of the modified MMSE detector in general settings. Hence, we study its performance in an ideal case. Consider one resource block as shown in Figure 5. We make the following assumptions: (i) the 12 subcarrier channels of this resource block are frequency-flat; (ii) the

Fig. 6: Rx Hardware configuration.

channel matrix $\mathbf{H}$ is full rank; (iii) the Rx has more antennas than the Jx has, i.e., $M > N$; (iv) the number of DMRS elements is not less than the number of jamming sources, i.e., $|\mathcal{R}| \geq N$; and (v) noise is zero, i.e., $\sigma_w = 0$. In this special case, we have the following lemma.

Lemma 1: In the above case, the modified MMSE detector in (20) *can perfectly decode the signal in the presence of jamming signals, i.e.,* $\hat{s}(l,k) = s(l,k)$, $\forall l, k$.

The proof is provided in Appendix A. We note that the assumption $|\mathcal{R}| \geq N$ always holds in practical mmWave communication systems. Here, N denotes the number of RF chains (i.e., digital channels, not the number of patch antenna elements) in a mmWave device, which is typically limited to two. Therefore, this assumption almost surely holds in practice. In what follows, we conduct experiments in realistic scenarios to evaluate the performance of this digital beamformer.

VII. Implementation

To evaluate the performance of our jamming-resistant mmWave Rx, we have built a mmWave testbed for demonstration and evaluation. Our testbed consists of three nodes: one Tx, one Jx, and one Rx, which we describe as follows.

Tx: The hardware of Tx includes a computer for data processing, a USRP X310 device for signal processing, and a Sivers EVK02004 for mmWave (28 GHz) signal transmission. We implemented the waveform and frame structure at the Tx using the PHY-layer code from srsRAN Project [43]. A simplified MAC layer was implemented to accept data packets from the upper-layer applications and modulate the data for signal transmission. All data process was done on the general computer using multi-thread implementation. The computer sends the processed I/Q data to USRP X310 via 10 Gbps Ethernet. USRP X310 up-converts the signal to IF (immediate frequency) at 3.5 GHz, which was sent to Sivers EVK02004 via differential SMA connectors. Sivers EVK02004 up-converts the 3.5 GHz IF signal to 28 GHz RF (radio frequency) signal for transmission via its phased-array antenna. The phased-array antenna has 16 (4×4) patch elements, which can be controlled electronically via a USB interface for analog beam steering. Sivers EVK02004 has two input connectors: one for horizontal polarization transmission, and the other for vertical polarization transmission. The IF signal from USRP X310 goes through a power divider (a passive device) to feed the two input connectors for both horizontal and vertical transmissions.

Jx: The Jx has a similar setup as the Tx. The only differences are: i) it uses USRP N210 rather than X310; ii) it transmits pseudo-noise, WiFi waveforms, and CDMA waveforms, rather than NR waveforms; iii) its transmission power is 10 dB stronger than the Tx's power. This was achieved through the gain control on Sivers EVK02004.

Rx: The Rx was built using a high-performance computer, USRP N310, and Sivers EVK02004. Different from the Tx, the Rx has two independent data streams from the same phased-array antenna (via horizontal and vertical polarization). In the general computer, we implemented the signal demodulation modules as well as our ABF and DBF algorithms to decode NR signal frames from the Tx, in the presence of a jamming signal. All the signal/data processing modules were implemented on the computer using C++ and multi-thread programming.

System Parameters: Due to the hardware limitation, the bandwidth of signal transmission is 20 MHz. The sampling rate is 30.72 MSps. The Tx's transmission power is about 15 dBm, while the Jx's transmission power is about 25 dBm. The phased-array antenna has 63 beam candidates for horizontal polarization and 63 beam candidates for vertical polarization. In total, there are 3,969 (63×63) analog beams for selection.

Real-Time Video streaming Demo: To show the robustness of our jamming-resistant Rx, we have created a demo video showing real-time video streaming in the presence of constant jamming signals. The demo can be found in [17].

VIII. Performance Evaluation

In this section, we conduct experiments to characterize the performance of our jamming-resilient Rx design in realistic scenarios. While our approach is generic, our experiments focus on the case where the network has a single Jx. We try to answer the following questions.

- **Q1 (Section VIII-B):** How many iterations are needed for BayOpt ABF in general? What is the performance loss of BayOpt ABF compared to exhaustive search?
- **Q2 (Section VIII-C):** What is the throughput gain of our modified MMSE DBF?
- **Q3 (Section VIII-D):** What is the throughput gain of our jamming-resistant Rx (i.e., ABF + DBF) in realistic scenarios?

A. Experimental Setup and Metrics

Experimental Setup: We deploy our testbed in four different scenarios as shown in Figure 7 to evaluate the performance of our jamming-resilient Rx. In each scenario, we place the three nodes (Tx, Jx, and Rx) at different locations for the measurement. Each scenario has 40 locations that have been tested. The Tx sends 5G NR signals using the frame structure shown in Figure 2. Unless stated otherwise, the Jx transmits pseudo-noise as the jamming signal.

Measurement Methodology and Metrics: We use three metrics to measure the performance of the proposed jamming-resistant Rx: signal-to-jamming power ratio (SJR), EVM, and throughput. SJR can be measured at the Rx by intentionally turning on/off Tx or Jx. This metric is used to characterize the performance of ABF at the Rx. EVM can be measured directly at the Rx. It characterizes the overall performance of

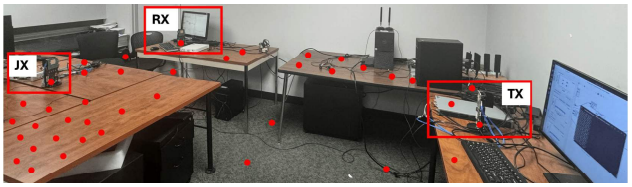

(a) Scenario 1: Office.

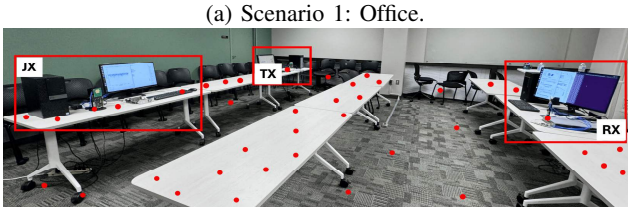

(b) Scenario 2: Conference room.

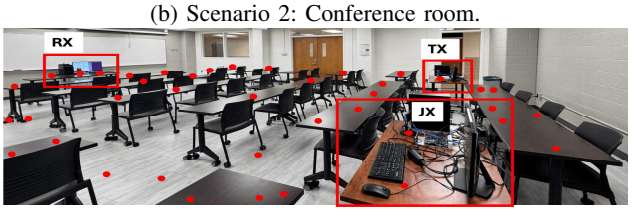

(c) Scenario 3: Classroom.

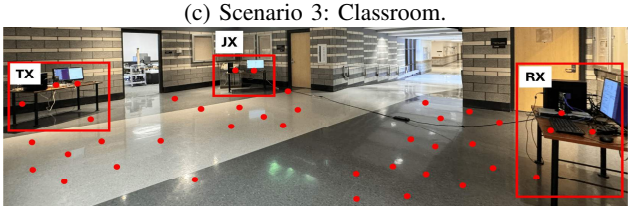

(d) Scenario 4: Hallway.

Fig. 7: Four scenarios for experimentation.

TABLE II: EVM-to-MCS mapping in a 5G network [45].

EVM (dB)	-2	-5	-10	-14	-16	-19	-20	-23	-26	-30	-33
Modulation order	2	2	6	6	6	6	8	8	8	10	10
Coding rate	1/3	2/3	1/3	1/2	2/3	5/6	2/3	5/6	8/9	13/14	17/18
Spectrum eff (bps/Hz)	2/3	4/3	2	3	4	5	16/3	20/3	64/9	65/7	85/9

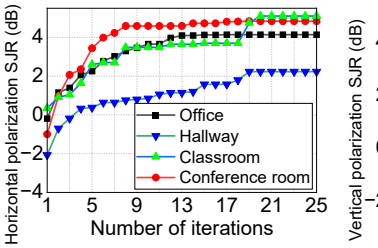

(a) SJR of horizontal polarization.

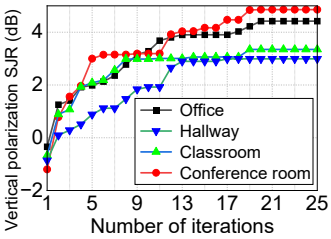

(b) SJR of vertical polarization.

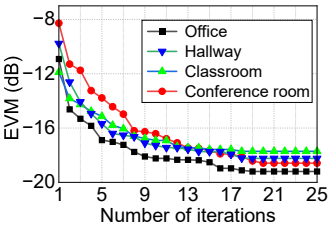

(c) EVM.

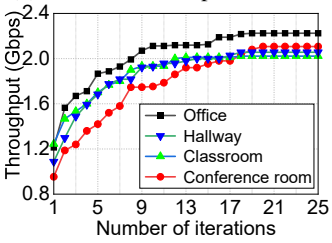

(d) Throughput.

Fig. 8: Rx's SJR, EVM, and throughput performance versus the number of BayOpt iterations for its ABF in four scenarios.

the communications except for the modulation and channel codes. In our experiments, it is challenging to measure the throughput directly on the testbed. This is because throughput measurement requires an accurate rate adaptation and retransmission mechanism, which requires tremendous engineering efforts to implement and calibrate. In light of this challenge, we use the measured EVM to estimate the throughput using the MCS table in Table II. Specifically, we calculate throughput as follows: $TP = BW \times \gamma(EVM)$, where BW=400MHz is the mmWave bandwidth, EVM is the measured value from experiments, $\gamma(\cdot)$ returns the best spectrum efficiency for a given EVM value shown in Table II.

EVM-to-Throughput Mapping: This table-lookup approach for throughput estimation has been widely used in the 4G/5G industry for system-level simulation [44]. The measured EVM already accounts for dynamic network factors such as transmission power, path loss, fast fading, noise, and interference levels. The resulting EVM-to-throughput value is determined by physical-layer techniques such as modulation and coding, and is therefore deterministic. This mapping is widely regarded as accurate and capable of providing high-fidelity performance evaluation.

B. Analog Beamforming (ABF)

The convergence speed of BayOpt is critical as it determines the communication overhead. In this part, we examine the convergence speed of our proposed BayOPT framework for ABF. Our aim is to answer the following two questions: i) how many iterations are needed for BayOpt to achieve its convergence? ii) what is its performance loss compared to exhaustive search? We first examine a case in each scenario, and then analyze extensive experimental data. Throughout our experiments in this part, the DBF is fixed.

Case studies: To understand how BayOpt converges, we select one case from each of the four scenarios shown in Figure 7. We examine the collected data to observe the Rx's performance (SJR, EVM, and throughput) versus the number of iterations in BayOpt. Figure 8 presents our experimental results. Recall that the Rx has two data streams from the phased-array antenna: one from horizontal polarization, and the other from vertical polarization. Figure 8(a) and (b) present the measured SJR of these two data streams versus the number of search iterations for ABF. It is evident that the SJR of both data streams increases when the number of iterations increases. This indicates the efficiency of BayOpt. Figure 8(c) and (d) present the measured EVM and throughput of the Rx, respectively. It can be seen that the EVM keeps decreasing, and the throughput keeps increasing, as the number of BayOpt iterations increases. The 25 iterations of the search for ABF almost double the Rx's throughput in all four scenarios. The measurement results show that 25 iterations are sufficient for BayOpt in this case.

Extensive Studies: We now extend the case studies to extensive measurement. For each of those four scenarios, we randomly choose 40 locations for Tx, Jx, and Rx. The orientation of their phased-array antenna is randomly adjusted but pointing to each other in general. For each case, we

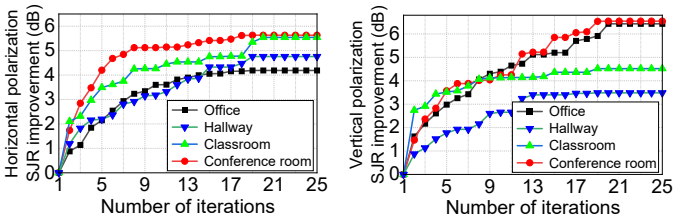

(a) SJR of horizontal polarization.

(b) SJR of vertical polarization.

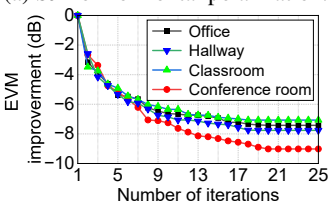

(c) EVM.

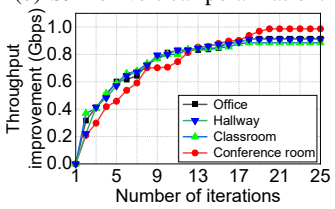

(d) Throughput.

Fig. 9: Average improvement of SJR, EVM, and throughput performance at each iteration of BayOpt.

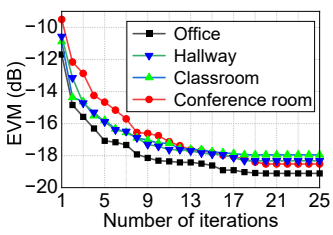

(a) EVM.

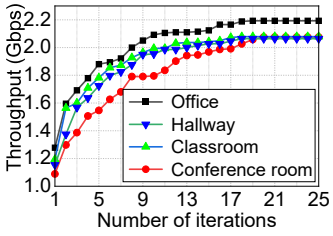

(b) Throughput.

Fig. 10: Average EVM and throughput performance over all locations in four scenarios.

record the SJR of two data streams and the EVM value in each iteration of BayOpt. We collect the improvement of SJR, EVM, and throughput in each iteration of BayOpt at each location of those four scenarios. For instance, the average improvement of EVM is expressed as $\Delta EVM(i) = \frac{1}{L}\sum_{1\le l\le L}\left[EVM_l(i) - EVM_l(1)\right]$, where $EVM_l(i)$ is the measured decibel EVM in the ith iteration of BayOpt at location l.

We plot the average improvement of SJR, EVM and throughput in Figure 9. It can be observed that as the number of iterations increases, the EVM decreases while the throughput increases. The average EVM is 7.85 dB, and the average throughput 0.93 Gbps.

In addition to the per-iteration improvement, we also calculate the average EVM and throughput of each BayOpt iteration. For instance, the average EVM is calculated as $EVM(i) = \frac{1}{L}\sum_{1\le l\le L} EVM_l(i)$, where i is iteration index. Figure 10 plots the average EVM and throughput versus the number of iterations. It can be seen that after 25 iterations throughput increases 72.6%, 90.6%, 74.1%, and 78.9% in office, conference room, classroom, and hallway, respectively.

EVM and Throughput Comparison: To characterize the performance of BayOpt, we compare it with two benchmarks: *Exhaustive search* and *Nelder-Mead search* [46]. In this comparison, BayOpt uses 25 iterations. In contrast, exhaustive search uses 3,969 iterations, and Nelder-Mead search uses

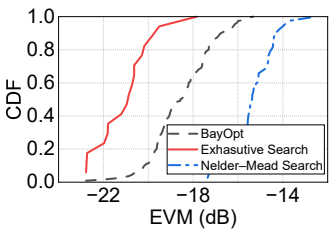

(a) EVM comparison.

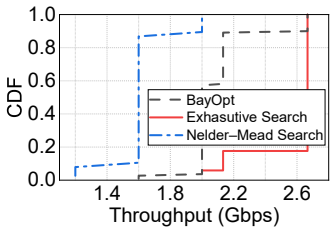

(b) Throughput comparison.

Fig. 11: Comparison of BayOpt with exhaustive search and Nelder-Mead Search.

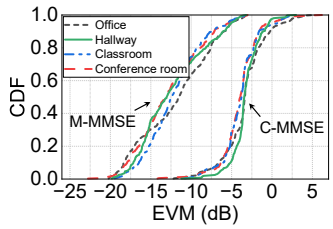

(a) EVM.

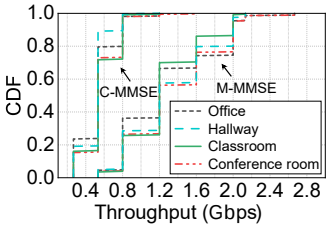

(b) Throughput.

Fig. 12: Performance comparison of M-MMSE DBF and C-MMSE DBF.

25 iterations. Figure 11 depicts our experimental results. We can observe that exhaustive search, BayOpt and Nelder-Mead Search can reach an average EVM of -20.97 dB, -18.51 dB, and -15.27 dB, respectively; and they achieve an average throughput of 2.67 Gbps, 2.13 Gbps, and 1.6 Gbps, respectively. BayOpt can achieve 80.0% throughput of exhaustive search while using only 0.6% search time of exhaustive search (25 search iterations versus 3,969 search iterations). Compared to BayOpt ABF, Nelder-Mead Search achieves 33.1% throughput gain when using the same number of search iterations.

C. Digital Beamforming (DBF)

To study the performance of its DBF, we fix the Rx's ABF and consider two cases: Modified MMSE for DBF [M-MMSE DBF, see Eqn (20)] and Conventional MMSE for DBF [C-MMSE DBF, see Eqn (16)]. In what follows, we first look into case studies and then present our extensive measurements.

Case Studies: To better understand DBF, we select one case from each of the four scenarios shown in Figure 7 to examine the performance of M-MMSE DBF in the comparison of C-MMSE DBF. Figure 12 presents the EVM and throughput distributions of M-MMSE DBF and C-MMSE DBF. The distribution is from the large number of beam directions used for ABF. It can be observed that M-MMSE DBF can achieve EVM with an average of -11.9 dB, -12.8 dB, -12.1 dB, and -12.4 dB in office, conference room, classroom, and hallway, respectively. Compared to C-MMSE DBF, M-MMSE DBF improves the EVM performance by 8.5 dB, 8.8 dB, 8.24 dB, and 9.1 dB respectively. M-MMSE can achieve throughput with an average of 1.29 Gbps, 1.37 Gbps, 1.26 Gbps, and 1.33 Gbps respectively. Compared to C-MMSE DBF, M-

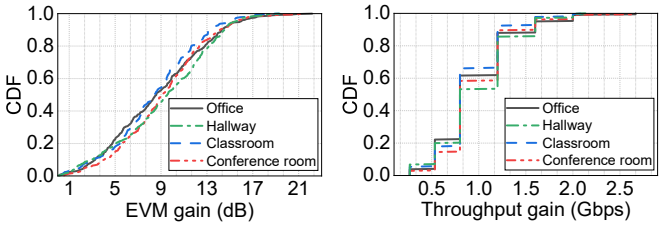

(a) EVM gain. (b) Throughput gain.

Fig. 13: Performance gain of M-MMSE DBF over C-MMSE DBF.

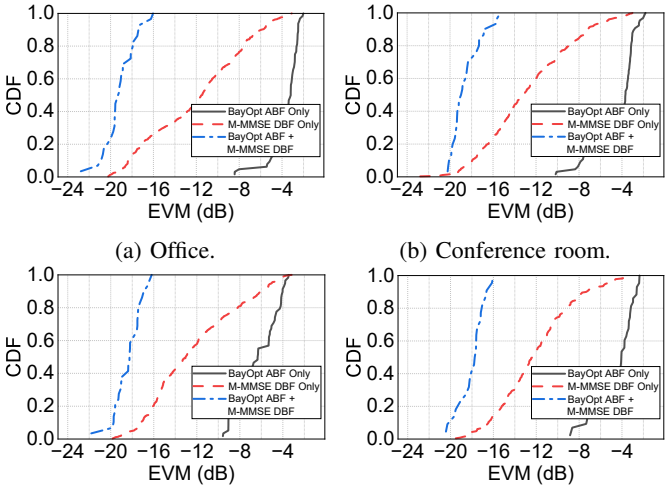

(a) Office. (b) Conference room.

(c) Hallway. (d) Classroom.

Fig. 14: EVM distribution in four scenarios.

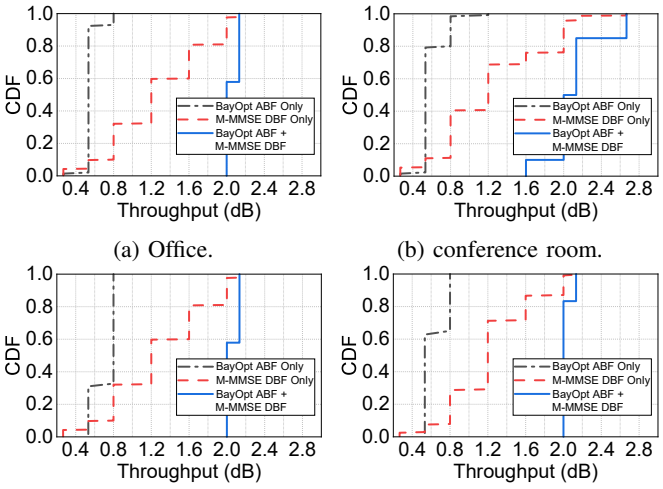

(a) Office. (b) conference room.

(c) Hallway. (d) Classroom.

Fig. 15: Throughput distribution in four scenarios.

TABLE III: Average performance under four scenarios.

	Office	Conf. room	Classroom	Hallway	Average
EVM (dB)					
BayOpt ABF Only	-3.54	-4.47	-6.54	-4.68	-4.81
M-MMSE DBF Only	-11.93	-12.76	-12.38	-12.10	-12.49
BayOpt ABF + M-MMSE DBF	-19.11	-18.52	-18.33	-17.96	-18.48
Throughput (Gbps)					
BayOpt ABF Only	0.55	0.59	0.63	0.71	0.62
M-MMSE DBF Only	1.31	1.23	1.22	1.28	1.26
BayOpt ABF + M-MMSE DBF	2.22	2.11	2.02	2.06	2.10

MMSE DBF increases the average throughput by 0.76 Gbps, 0.8 Gbps, 0.69 Gbps, and 0.82 Gbps respectively.

Extensive Studies: For extensive study of DBF performance, we measured EVM difference in the four scenarios as shown in Figure 7. The Tx, Jx, and Rx nodes were placed at different locations and faced to different directions. Figure 13 shows the DBF performance from our extensive studies. We observed that, compared to C-MMSE, M-MMSE DBF improves the average EVM performance by 9.0 dB and increases the average throughput by 0.96 Gbps.

D. Overall Performance

After examining the performance of BayOpt ABF and M-MMSE DBF individually, we now study the overall performance of our proposed anti-jamming Rx by combining ABF and DBF together. Meanwhile, we conduct an ablation study to evaluate the performance gains of BayOpt ABF and M-MMSE DBF individually. Again, we use EVM and throughput as the performance metrics.

Figure 14 presents the EVM distribution in the four scenarios when ABF and DBF are separately and jointly used. It can be seen that both BayOpt ABF and M-MMSE DBF significantly decrease the EVM at the Rx. Specifically, M-MMSE DBF decreases the Rx's EVM by an average of 7.68 dB; and BayOpt ABF decreases the Rx's EVM by an average of 5.99 dB. The combination of BayOpt ABF and M-MMSE DBF decreases the Rx's EVM by an average of 13.67 dB.

Figure 15 presents the Rx's throughput distribution in the four scenarios. It can be seen that, while using either BayOpt ABF or M-MMSE DBF can achieve a certain amount of throughput gain, the combination of these two techniques can significantly improve the throughput in the presence of jamming signal. This reveals the efficiency of our holistic anti-jamming solution for a mmWave Rx. Numerically, M-MMSE DBF improves the average throughput by 0.84 Gbps; and BayOpt ABF improves the Rx's average throughput by 0.64 Gbps. The combination of these two techniques can improve the throughput by 1.48 Gbps. Table III summarizes the Rx's average EVM and throughput in the four scenarios.

It can be seen that the throughput CDF of our holistic algorithm (BayOpt ABF + M-MMSE DBF) in Figure 15 is not widely spread. This is because the proposed jamming mitigation algorithm is effective in most cases, due to two main factors: (i) mmWave signals do not propagate like laser beams; our measurements show that multipath and reflection are common in indoor environments; and (ii) the mmWave receiver has 16 antenna elements, each supporting both horizontal and vertical polarization, resulting in 32 effective channels for signal combining and jamming mitigation. One might expect the algorithm to be ineffective when the transmitter and jammer are located in the same direction relative to the receiver. However, we did not observe this phenomenon in

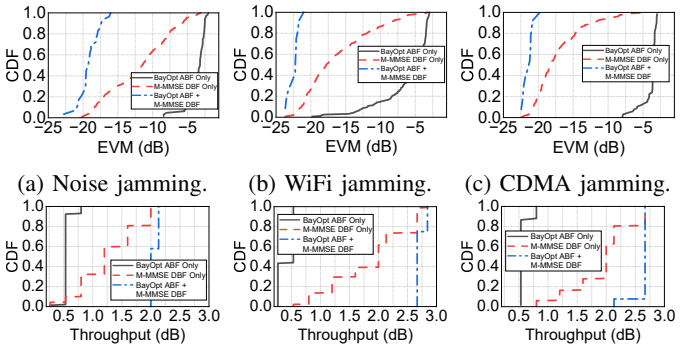

(a) Noise jamming. (b) WiFi jamming. (c) CDMA jamming.

(d) Noise jamming. (e) WiFi jamming. (f) CDMA jamming.

Fig. 16: EVM and throughput distribution when the Jx uses different jamming waveforms.

our experiments. We attribute this to the short wavelength of mmWave signals, the availability of 32 antenna elements, and the strong multipath effects in indoor scenarios.

Different Jamming Waveforms: To fully understand the jamming mitigation capability of our proposed Rx, we evaluate its performance when the Jx uses different jamming waveforms: pseudo-noise, WiFi, and CDMA. Following the same token, we evaluate the performance of BayOpt ABF and M-MMSE DBF techniques separately and jointly to characterize their individual and overall performances. Figure 16 illustrates the effectiveness of our proposed Rx against various jamming waveforms. Notably, BayOpt ABF and M-MMSE DBF significantly enhance performance, reducing the EVM by 15.57 dB, 16.23 dB, and 17.47 dB for pseudo-noise, WiFi, and CDMA jamming waveforms, respectively. Additionally, throughput improvements of 1.67 Gbps, 2.30 Gbps, and 2.03 Gbps are observed for the same waveforms. Figure 17 demonstrates the DBF performance, highlighting that M-MMSE DBF yields EVM gains of 8.78 dB, 12.34 dB, and 15.91 dB, alongside throughput enhancements of 0.96 Gbps, 1.34 Gbps, and 1.79 Gbps. These results affirm the proposed anti-jamming Rx's capability to counteract diverse jamming strategies, thereby underscoring its potential in facilitating spectrum sharing.

Comparison with Jamming-free Case: Above we presented the EVM and throughput performance of our proposed anti-jamming Rx in the scenarios where Jx transmits 10 dB stronger signals than Tx. Here, we conduct experiments for the following performance comparison: i) the proposed Rx in jamming scenarios; and ii) a conventional Rx in jamming-free scenarios. To measure the performance of a conventional Rx in jamming-free scenarios, we use its two RF chains for spatial diversity. That is, the Tx sends one data stream to the Rx; the Rx uses maximum ratio combination as its DBF for signal demodulation. Additionally, the Rx uses BayOpt ABF to identify its best analog beam index within 25 iterations. Figure 18 presents the measured EVM and throughput in four scenarios. It can be seen that our proposed Rx under jamming attack can achieve 73.7%, 71.7%, 71.9%, and 74.9% throughput compared to the conventional Rx in jamming-free scenarios. The results show that the proposed Rx is efficient in salvaging mmWave communications in the presence of jamming attacks.

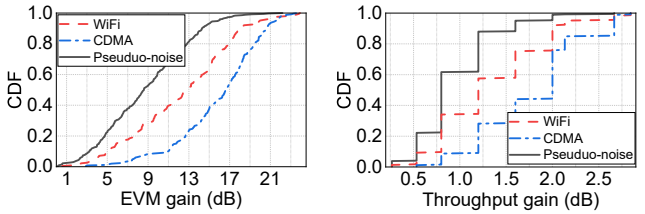

(a) EVM gain. (b) Throughput gain.

Fig. 17: EVM and throughput gain of M-MMSE DBF over C-MMSE DBF in different waveforms.

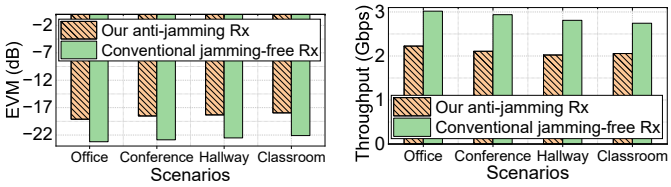

(a) EVM Comparison. (b) Throughput Comparison.

Fig. 18: EVM and throughput comparison of jamming-present over jamming-free cases.

IX. Concluding Remarks

In this paper, we presented a joint ABF and DBF scheme for a mmWave Rx to enable jamming-resilient mmWave communications by leveraging the polarization diversity of phased-array antennas. The beamforming scheme comprises two key techniques: a BayOpt framework for ABF, and an M-MMSE detector for DBF. The combination of these techniques enables an Rx to suppress jamming signals in both analog and digital domain, making it capable of decoding data packets in the presence of jamming signals. Extensive over-the-air experiments confirm the effectiveness and efficiency of those two techniques, and also demonstrated the jamming resilience of the mmWave Rx.

This work focuses on addressing constant jamming attacks. To extend the proposed anti-constant-jamming solution to counter reactive and cognitive jamming, it is essential to incorporate adaptability, unpredictability, and rapid response mechanisms. Rapid jammer detection can be achieved by monitoring real-time link metrics, such as error rates or signal subspace changes, and triggering immediate adaptation when shifts are observed. Analog beamforming can be enhanced with time-aware optimization techniques, such as sliding-window Bayesian optimization or contextual bandits, to quickly re-select beams under changing jamming conditions. Digital beamforming should evolve from batch to online or recursive updates, enabling real-time suppression of adaptive jamming signals through subspace tracking or blind separation methods.

Appendix A
Proof of Lemma 1

Given that $M > N$, $\mathbf{H}$ is a square or tall/thin matrix. Moreover, $\mathbf{H}$ in real systems is always of full column rank. Then, based on (20), we have:

$$\vec{p}^{\top} = \mathcal{F}\{\mathbf{P}\}$$

$$
\begin{aligned}
&\overset{(a)}{=} \Big[\sum_{(l,k)\in\mathcal{R}} s(l,k)\vec{y}(l,k)^{\mathsf{H}}\Big]\Big[\sum_{(l,k)\in\mathcal{R}} \vec{y}(l,k)\vec{y}(l,k)^{\mathsf{H}}\Big]^{\dagger}\\
&\overset{(b)}{=} \Big[\sum_{(l,k)\in\mathcal{R}} s(l,k)\vec{x}(l,k)^{\mathsf{H}}\mathbf{H}^{\mathsf{H}}\Big]\Big[\sum_{(l,k)\in\mathcal{F}} \mathbf{H}\vec{x}(l,k)\vec{x}(l,k)^{\mathsf{H}}\mathbf{H}^{\mathsf{H}}\Big]^{\dagger}\\
&\overset{(c)}{=} \Big[\mathcal{F}\{\hat{\mathbf{R}}_{\mathbf{x}}\}\mathbf{H}^{\mathsf{H}}\Big]\Big[\mathbf{H}\hat{\mathbf{R}}_{\mathbf{x}}\mathbf{H}^{\mathsf{H}}\Big]^{\dagger}\\
&\overset{(d)}{=} \mathcal{F}\Big\{\big[\hat{\mathbf{R}}_{\mathbf{x}}\mathbf{H}^{\mathsf{H}}\big]\big[\mathbf{H}\hat{\mathbf{R}}_{\mathbf{x}}\mathbf{H}^{\mathsf{H}}\big]^{\dagger}\Big\}\\
&\overset{(e)}{=} \mathcal{F}\Big\{\hat{\mathbf{R}}_{\mathbf{x}}\mathbf{H}^{\mathsf{H}}\big[\mathbf{H}^{\mathsf{H}}\big]^{\dagger}\hat{\mathbf{R}}_{\mathbf{x}}^{\dagger}\mathbf{H}^{\dagger}\Big\}\\
&\overset{(f)}{=} \mathcal{F}\big\{\mathbf{H}^{\dagger}\big\},
\end{aligned}
\tag{21}
$$

where (a) follows from (20); (b) follows from the fact that $\vec{y} = \mathbf{H}\vec{x}$ when $\sigma_w = 0$; (c) follows from our definition that $\hat{\mathbf{R}}_x = \sum_{(l,k)\in\mathcal{R}} \vec{x}(l,k)\vec{x}(l,k)^{\mathsf{H}}$; (d) follows from that fact that the operator $\mathcal{F}\{\cdot\}$ can be extended to include more terms; (e) and (f) follow from the fact that $\mathbf{H}$ is a square or tall matrix of full rank.

Based on (21), we have

$$
\begin{aligned}
\hat{s}(l,k) &= \vec{p}^{\top}\vec{y}(l,k) = \mathcal{F}\big\{\mathbf{H}^{\dagger}\big\}\vec{y}(l,k)\\
&= \mathcal{F}\big\{\mathbf{H}^{\dagger}\big\}\mathbf{H}\vec{x}(l,k) = \mathcal{F}\big\{\vec{x}(l,k)\big\} = s(l,k).
\end{aligned}
\tag{22}
$$

This completes our proof.

REFERENCES

[1] F. Liu, M. W. Marcellin, N. A. Goodman, and A. Bilgin, "Compressive sampling for detection of frequency-hopping spread spectrum signals," *IEEE Transactions on Signal Processing*, vol. 64, no. 21, pp. 5513–5524, 2016.

[2] Z. Yao, F. Guo, J. Ma, and M. Lu, "Orthogonality-based generalized multicarrier constant envelope multiplexing for dsss signals," *IEEE Transactions on Aerospace and Electronic Systems*, vol. 53, no. 4, pp. 1685–1698, 2017.

[3] K. Firouzbakht, G. Noubir, and M. Salehi, "On the performance of adaptive packetized wireless communication links under jamming," *IEEE Transactions on Wireless Communications*, vol. 13, no. 7, pp. 3481–3495, 2014.

[4] R. George and T. A. J. Mary, "Review on directional antenna for wireless sensor network applications," *IET Communications*, vol. 14, no. 5, pp. 715–722, 2020.

[5] A. Toma, A. Krayani, M. Farrukh, H. Qi, L. Marcenaro, Y. Gao, and C. S. Regazzoni, "Ai-based abnormality detection at the phy-layer of cognitive radio by learning generative models," *IEEE Transactions on Cognitive Communications and Networking*, vol. 6, no. 1, pp. 21–34, 2020.

[6] J. Ye, A. Kammoun, and M.-S. Alouini, "Reconfigurable intelligent surface enabled interference nulling and signal power maximization in mmwave bands," *IEEE Transactions on Wireless Communications*, vol. 21, no. 11, pp. 9096–9113, 2022.

[7] Y. Sun, Y. Zhu, K. An, G. Zheng, S. Chatzinotas, K.-K. Wong, and P. Liu, "Robust design for ris-assisted anti-jamming communications with imperfect angular information: A game-theoretic perspective," *IEEE Transactions on Vehicular Technology*, vol. 71, no. 7, pp. 7967–7972, 2022.

[8] H. Pirayesh and H. Zeng, "Jamming attacks and anti-jamming strategies in wireless networks: A comprehensive survey," *IEEE communications surveys & tutorials*, vol. 24, no. 2, pp. 767–809, 2022.

[9] Y. Zhang, Y. Shen, X. Jiang, and S. Kasahara, "Secure millimeter-wave ad hoc communications using physical layer security," *IEEE Transactions on Information Forensics and Security*, vol. 17, pp. 99–114, 2022.

[10] T. T. Do, E. Björnson, E. G. Larsson, and S. M. Razavizadeh, "Jamming-resistant receivers for the massive mimo uplink," *IEEE Transactions on Information Forensics and Security*, vol. 13, no. 1, pp. 210–223, 2018.

[11] Y. Cai, C. Zhao, Q. Shi, G. Y. Li, and B. Champagne, "Joint beamforming and jamming design for mmwave information surveillance systems," *IEEE Journal on Selected Areas in Communications*, vol. 36, no. 7, pp. 1410–1425, 2018.

[12] M. V. Jamali and H. Mahdavifar, "Covert millimeter-wave communication: Design strategies and performance analysis," *IEEE Transactions on Wireless Communications*, vol. 21, no. 6, pp. 3691–3704, 2022.

[13] Z. Wang, Q. Liu, M. Li, and W. Kellerer, "Energy efficient analog beamformer design for mmwave multicast transmission," *IEEE Transactions on Green Communications and Networking*, vol. 3, no. 2, pp. 552–564, 2019.

[14] Y. Long, Z. Chen, J. Fang, and C. Tellambura, "Data-driven-based analog beam selection for hybrid beamforming under mm-wave channels," *IEEE Journal of Selected Topics in Signal Processing*, vol. 12, no. 2, pp. 340–352, 2018.

[15] L. Jiang and H. Jafarkhani, "Multi-user analog beamforming in millimeter wave mimo systems based on path angle information," *IEEE Transactions on Wireless Communications*, vol. 18, no. 1, pp. 608–619, 2019.

[16] X. Li, Y. Zhu, and P. Xia, "Enhanced analog beamforming for single carrier millimeter wave mimo systems," *IEEE Transactions on Wireless Communications*, vol. 16, no. 7, pp. 4261–4274, 2017.

[17] INSS Lab, Michigan State University, "Anti-Jamming mmWave System Demonstration Video." https://inss.egr.msu.edu/videos/ajmmwave.mp4, 2025. Accessed: 2025-05-19.

[18] S. Zhang, B. Ji, K. Zeng, and H. Zeng, "Realizing uplink mu-mimo communication in mmwave wlans: Bayesian optimization and asynchronous transmission," in *IEEE Conference on Computer Communications*, pp. 1–10, 2023.

[19] M. Scalabrin, G. Bielsa, A. Loch, M. Rossi, and J. Widmer, "Machine learning based network analysis using millimeter-wave narrow-band energy traces," *IEEE Transactions on Mobile Computing*, vol. 19, no. 5, pp. 1138–1155, 2020.

[20] S. Dinh-Van, T. M. Hoang, B. B. Cebecioglu, D. S. Fowler, Y. K. Mo, and M. D. Higgins, "A defensive strategy against beam training attack in 5g mmwave networks for manufacturing," *IEEE Transactions on Information Forensics and Security*, vol. 18, pp. 2204–2217, 2023.

[21] Q. Xue, Y.-J. Liu, Y. Sun, J. Wang, L. Yan, G. Feng, and S. Ma, "Beam management in ultra-dense mmwave network via federated reinforcement learning: An intelligent and secure approach," *IEEE Transactions on Cognitive Communications and Networking*, vol. 9, no. 1, pp. 185–197, 2023.

[22] C. Liu, M. Li, L. Zhao, P. Whiting, S. V. Hanly, and I. B. Collings, "Millimeter-wave beam search with iterative deactivation and beam shifting," *IEEE Transactions on Wireless Communications*, vol. 19, no. 8, pp. 5117–5131, 2020.

[23] S. Kumar, S. Suman, and S. De, "Dynamic resource allocation in uav-enabled mmwave communication networks," *IEEE Internet of Things Journal*, vol. 8, no. 12, pp. 9920–9933, 2021.

[24] Y. Cao, S. Wang, M. Jin, N. Zhao, Y. Chen, Z. Ding, and X. Wang, "Joint user grouping and power optimization for secure mmwave-noma systems," *IEEE Transactions on Wireless Communications*, vol. 21, no. 5, pp. 3307–3320, 2022.

[25] H. Nosrati, E. Aboutanios, and D. Smith, "Multi-stage antenna selection for adaptive beamforming in mimo radar," *IEEE Transactions on Signal Processing*, vol. 68, pp. 1374–1389, 2020.

[26] H. Yang, Z. Xiong, J. Zhao, D. Niyato, Q. Wu, H. V. Poor, and M. Tornatore, "Intelligent reflecting surface assisted anti-jamming communications: A fast reinforcement learning approach," *IEEE Transactions on Wireless Communications*, vol. 20, no. 3, pp. 1963–1974, 2021.

[27] J. Liu, G. Yang, Y.-C. Liang, and C. Yuen, "Max-min fairness in ris-assisted anti-jamming communications: Optimization versus deep reinforcement learning approaches," *IEEE Transactions on Communications*, pp. 1–1, 2024.

[28] P. Zhang, J. Dong, J. He, J. Liu, and F. Xiao, "Adaptive jamming attack detection under noise uncertainty in mmwave massive mimo systems," *IEEE Transactions on Vehicular Technology*, vol. 72, no. 7, pp. 9002–9016, 2023.

[29] X. Yuan, S. Hu, W. Ni, R. P. Liu, and X. Wang, "Joint user, channel, modulation-coding selection, and ris configuration for jamming resistance in multiuser ofdma systems," *IEEE Transactions on Communications*, vol. 71, no. 3, pp. 1631–1645, 2023.

[30] W. Bai, X. Zou, P. Li, J. Ye, Y. Yang, L. Yan, W. Pan, and L. Yan, "Photonic millimeter-wave joint radar communication system using spectrum-spreading phase-coding," *IEEE Transactions on Microwave Theory and Techniques*, vol. 70, no. 3, pp. 1552–1561, 2022.

[31] B. Okyere, L. Musavian, B. Özbek, S. A. Busari, and J. Gonzalez, "The resilience of massive mimo pnc to jamming attacks in vehicular networks," *IEEE Transactions on Intelligent Transportation Systems*, vol. 22, no. 7, pp. 4110–4117, 2021.

[32] X. Wu, J. Ma, C. Gu, X. Xue, and X. Zeng, "Robust secure transmission design for irs-assisted mmwave cognitive radio networks," *IEEE Transactions on Vehicular Technology*, vol. 71, no. 8, pp. 8441–8456, 2022.

[33] X. Qi, M. Peng, H. Zhang, and X. Kong, "Anti-jamming hybrid beamforming design for millimeter-wave massive mimo systems," *IEEE Transactions on Wireless Communications*, pp. 1–1, 2024.

[34] D. Darsena and F. Verde, "Anti-jamming beam alignment in millimeter-wave mimo systems," *IEEE Transactions on Communications*, vol. 70, no. 8, pp. 5417–5433, 2022.

[35] G. Asemian, M. Amini, and B. Kantarci, "Active ris-noma uplink in urllc, jamming mitigation via surrogate and deep learning," *IEEE Open Journal of the Communications Society*, 2025.

[36] D. Ramasamy, S. Venkateswaran, and U. Madhow, "Compressive tracking with 1000-element arrays: A framework for multi-gbps mm wave cellular downlinks," in *2012 50th Annual Allerton Conference on Communication, Control, and Computing (Allerton)*, pp. 690–697, IEEE, 2012.

[37] H. Hassanieh, O. Abari, M. Rodriguez, M. Abdelghany, D. Katabi, and P. Indyk, "Fast millimeter wave beam alignment," in *Proceedings of the 2018 Conference of the ACM Special Interest Group on Data Communication*, pp. 432–445, 2018.

[38] J. Mockus, *Bayesian approach to global optimization: theory and applications*, vol. 37. Springer Science & Business Media, 2012.

[39] C. K. Williams and C. E. Rasmussen, *Gaussian processes for machine learning*, vol. 2. MIT press Cambridge, MA, 2006.

[40] J. Snoek, H. Larochelle, and R. P. Adams, "Practical bayesian optimization of machine learning algorithms," *Advances in neural information processing systems*, vol. 25, 2012.

[41] N. Stander and K. Craig, "On the robustness of a simple domain reduction scheme for simulation-based optimization," *Engineering Computations*, vol. 19, no. 4, pp. 431–450, 2002.

[42] J. Quinonero-Candela, C. E. Rasmussen, and C. K. Williams, "Approximation methods for gaussian process regression," in *Large-scale kernel machines*, pp. 203–223, MIT Press, 2007.

[43] srsRAN Project, "Open source O-RAN 5G CU/DU solution from Software Radio Systems (SRS)." https://github.com/srsran/srsran_project, 2023. Accessed on October-1-2023.

[44] S. Lagen, K. Wanuga, H. Elkotby, S. Goyal, N. Patriciello, and L. Giupponi, "New radio physical layer abstraction for system-level simulations of 5g networks," in *ICC 2020-2020 IEEE International Conference on Communications (ICC)*, pp. 1–7, IEEE, 2020.

[45] J. H. Bae, A. Abotabl, H.-P. Lin, K.-B. Song, and J. Lee, "An overview of channel coding for 5g nr cellular communications," *APSIPA transactions on signal and information processing*, vol. 8, p. e17, 2019.

[46] M.-M. Zhao, Y. Cai, M.-J. Zhao, Y. Xu, and L. Hanzo, "Robust joint hybrid analog-digital transceiver design for full-duplex mmwave multicell systems," *IEEE Transactions on Communications*, vol. 68, no. 8, pp. 4788–4802, 2020.